Combined Image Processing and Equivalent Circuit Approach for the Diagnostic of Atmospheric Pressure DBD

Vanesa Rueda, Rafael Diez, Nicolas Bente, Hubert Piquet

applied sciences

MDPI

Article

Combined Image Processing and Equivalent Circuit Approach for the Diagnostic of Atmospheric Pressure DBD

Vanesa Rueda [1,2], Rafael Diez [2,*], Nicolas Bente [1] and Hubert Piquet [1,*]

[1] LAPLACE Laboratory, Université de Toulouse, CNRS, INPT, UPS, 2 rue Charles Camichel, BP 7122, CEDEX 7, 31071 Toulouse, France
[2] Department of Electronics Engineering, Pontificia Universidad Javeriana, Bogota 110231, Colombia
* Correspondence: rdiez@javeriana.edu.co (R.D.); hubert.piquet@laplace.univ-tlse.fr (H.P.)

Abstract: The framework of this paper is the study of gas treatments (NOx abatement) by dielectric barrier discharge (DBD) at atmospheric pressure. To investigate the impact of various solutions for electrical energy injection on the treatment process, two diagnostic methods are considered to evaluate the discharging ratio on the reactor surface: an image processing method and a DBD equivalent circuit analysis, both presented in this paper. For the image analysis, the discharge area is first translated into gray levels, then segmented using the Otsu's method in order to perform the discharging ratio diagnostic. The equivalent circuit approach, derived from the classical Manley's diagram analysis, includes the behavior of the part of the reactor in which no discharge is happening. The identification of its parameters is used to estimate the discharging ratio, which evaluates the percentage of the reactor surface covered by the discharge. Experimental results with specifically developed power supplies are presented: they show a good agreement between the two methods. To allow a quantitative comparison of the discharge uniformity according to the operating conditions, the statistical analysis of gray level distribution is performed: non-uniform discharges with intense energy channels are shown to be clearly distinguished from more diffuse ones.

Keywords: dielectric barrier discharge; partial surface discharging; discharging ratio; image processing; equivalent circuit; Manley diagram; NOx abatement; DBD diagnostic; atmospheric pressure; discharge uniformity

Citation: Rueda, V.; Diez, R.; Bente, N.; Piquet, H. Combined Image Processing and Equivalent Circuit Approach for the Diagnostic of Atmospheric Pressure DBD. *Appl. Sci.* **2022**, *12*, 8009. https://doi.org/10.3390/app12168009

Academic Editor: Bogdan-George Rusu

Received: 8 July 2022
Accepted: 8 August 2022
Published: 10 August 2022

1. Introduction

Non-Thermal Plasma (NTP) are broadly used for applications such as ozone generation, treatment of surfaces, medical treatments, disinfection, and UV production [1–6]. In recent years, NTP has also become a rising technology for environmental protection. Many studies have reported effective removal of pollutants such as nitrogen oxides (NOx), sulfur dioxide (SO_2), carbon dioxide (CO_2), particulate matter, and volatile organic compounds (VOC) [1,7], with treatments usually processed at atmospheric pressure.

Dielectric Barrier Discharges (DBDs) are NTP produced in reactors, including at least one insulating layer between two metallic electrodes. In comparison with other NTP reactors, such as corona discharges and electron beams, DBDs are characterized by the absence of sparks, thanks to the dielectric barriers which limit the local current rise and by the possibility of obtaining uniform discharges, where the NTP covers the entire surface of the reactors, guaranteeing a quality treatment.

DBDs operate in filamentary or homogeneous mode [8,9]. In the homogeneous mode, the plasma is uniform and diffuse [1,8] and it presents a glowing aspect. For some applications, it has been proven to improve the process: for instance, thin films deposit requires homogeneous discharges in order to obtain a uniform treatment and prevent local damage on the treated surface [2]. The filamentary mode is characterized by streamers, intense energy channels distributed over the electrodes surface, randomly, or sometimes following

geometrical patterns [10]. Ozone generation, UV emission for instance, benefits from this mode. At atmospheric pressure, DBD generally operates in filamentary mode, and offer capabilities to initiate very valuable chemical transformations. According to their highly desirable characteristics, DBDs and packed-bed DBDs are widely used for pollutant removal applications. This is the case for the prospective application of our studies (NOx abatement) [7].

Experimental conditions such as the reactor geometry, materials, gas mixture, pressure, and electrical supply waveforms not only influence the discharge mode, but also the characteristics of the power injection into the plasma and the full or partial coverage of the reactor's surface by the NTP. Obtaining operating conditions where the surface of the reactor is fully covered by the plasma is indeed highly desirable for gas treatments: it means that each volume of the gas injected into the reactor will receive the effect of NTP treatment, contrary to the situation where only part of the reactor's surface is covered by the NTP, and thus part of the flowing gas may not receive the expected treatment. Such opposite situations are shown in Figure 1 (side view of a cylindrical reactor, detailed in Section 2, showing the streamers distribution seen through the transparent walls made with quartz).

Figure 1. Typical discharge appearance with partial discharging and different β percentages (white frame showing the limits of the reactor).

The partial discharging is quantified by the β (no units) percentage, which takes the 1 value when the surface is fully covered and 0 value when the discharge is OFF [8,11,12]. Among the diagnostic criteria used for the diagnostic of NTP delivered by DBD, this β discharging ratio is very important to improve the understanding of the efficiency of the gas treatments (NOx abatement in our case).

Different diagnostic methods of the discharge mode, based on its appearance, have been proposed. Ref. [9] introduced a simple method that detects the homogeneous glow discharge using the Manley figure and the voltage and current waveforms. This method is based on a definition of the homogeneous APGD (Atmospheric Pressure Glow Discharge), where only one current pulse per voltage half-cycle is generated. Other diagnostic methods include Intensified Charge-Coupled Device (ICCD), high-speed imaging, optical emission spectrum, numerical simulations, and image processing [13].

Given that the image processing method is effective, simple, and does not require expensive equipment, it is a good solution to analyze the discharges under different experimental conditions. However, if the aim is to detect the conventional glow discharge (APGD), it can only be used with short exposure time (~10 ns, which requires an expensive camera). When higher exposure times are used, the filaments cannot be always distinguished. Nevertheless, the image processing can be still used to analyze the uniformity of the discharge: in this paper an image processing algorithm is set up to study the uniformity of the discharges rather than the discharge mode (homogeneous or filamentary). This analysis of the discharge uniformity is based on the image gray level histogram [13] and produces, as a result, an estimation of the β partial discharging ratio. Additional statistical analysis of the images also allows a quantified comparison of the uniformity of the discharges.

Other diagnostics of DBD systems can be also achieved on the basis of measured electrical waveforms. Using these measurements, it is possible to identify the parameters of the well-known Manley diagram [14] and its associated DBD's equivalent circuit [15].

Originally based on the assumption that the discharge is uniform (with parameters of the equivalent circuit corresponding to a full use of the surface of the electrodes, i.e., $\beta = 1$), this approach can be simply extended [8,16] to consider partial discharging situation.

In order to implement complementary approaches for diagnostic of the discharges obtained in a DBD reactor for NOx abatement studies, the two aforementioned approaches (image processing and equivalent circuit) are considered in this paper. The article is organized as follows: Section 2 presents first the reactor, the power supply and the experimental test-bench, for which measurements are used in this paper. Then, the image processing algorithm for diagnostic with estimation of the β percentage of the surface covered by the discharge is detailed. Finally, the equivalent circuit, considering partial discharging phenomenon and the identification of its parameters (chiefly the β ratio) using the electrical measured waveforms, is presented.

In Section 3, the application of the two methods at different operating conditions obtained with the test-bench is proposed and the correspondence between the obtained β percentage values is discussed.

2. Materials and Methods

2.1. Experimental Setup

The schematic diagram of the experimental setup is presented in Figure 2. The system consists of a DBD reactor, a gas blending system, a power supply, measurement instruments, and the control interface:

- The reactor has a coaxial cylindrical geometry made up of quartz. The inner electrode is a stainless-steel foil, and the outer electrode is a metallic mesh (knitted thin wires made of tinned copper steel, usually used for EMI/RFI shielding of cables [17]) wrapped around the quartz tube. The diameter of the outer dielectric is 28 mm, and the diameter of the inner dielectric is 22 mm. The length of the mesh is 60 mm. Detailed dimensions are given in Figure 2.
- The feed-gas stream is composed of NO and N_2 and flows through the DBD reactor. The gas composition and total flow rate are adjustable. Two mass flow controllers (Bronkhorst EL-FLOW Prestige) are used to measure and regulate them. Presented results are for 3 lpm flow, with a NO concentration of 800 ppm.
- The DBD voltage is measured with a 200 MHz digital oscilloscope (LeCroy HDO4024) connected through a 1000:1 voltage probe (Testec TT-SI 9010), and the current is measured using a current probe (LeCroy AP015). The NO and NO_2 concentrations are obtained by the gas analyzer (Testo 350).

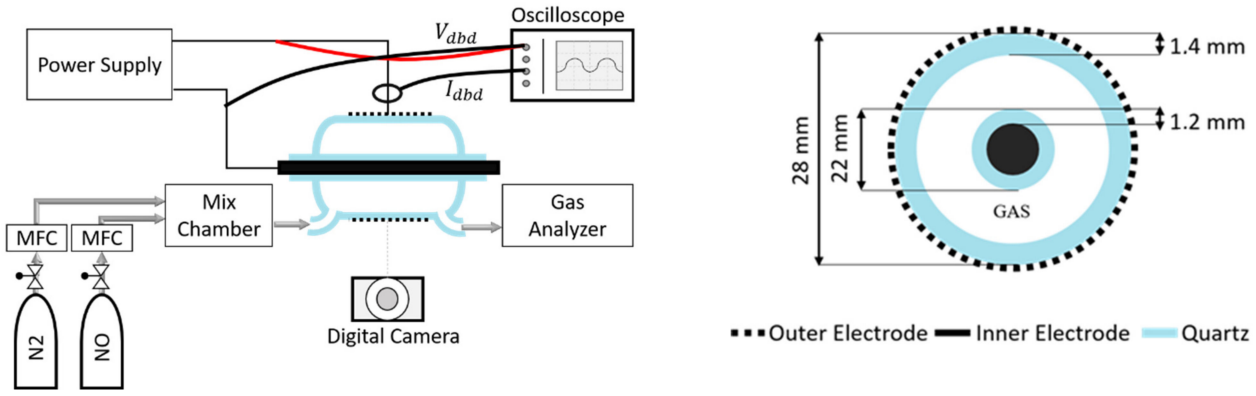

(**a**) (**b**)

Figure 2. Experimental setup (**a**) and reactor dimensions (**b**).

Two different electrical supplies are used for the experimentations: a sinusoidal voltage source and a square current source. The sinusoidal voltage waveforms (Figure 3b) are generated by a function generator connected to an audio amplifier. Since the output voltage

of the amplifier is too low to ignite a discharge, the amplifier output is connected to a high-voltage transformer. Frequency and peak voltage are the degrees of freedom made available by this supply: a maximum frequency of 20 kHz and a maximum voltage of 12 kV can be generated.

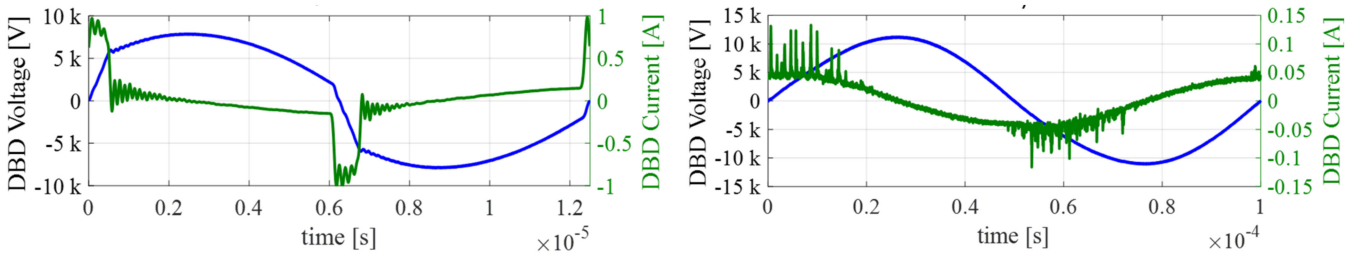

(**a**) (**b**)

Figure 3. Typical electrical waveforms (v_{DBD}, blue and i_{DBD}, green): (**a**) Square Current Source: here, *fsw* = 80 kHz, *J* = 1 A, *d* = 10%. (**b**) Sinusoidal Voltage Source: here, v_{DBD_peak} = 11.2 kV, *f* = 10 kHz.

A specific power supply has been also developed to create the plasma and to control the energy injected into the NTP. This one delivers square current waveforms (Figure 3a), which is generated by the power converter presented in [18,19]. This converter consists of a DC current source connected in cascade with a full-bridge current inverter and a step-up transformer. The converter delivers current pulses, whose shape is controlled by three degrees of freedom: frequency *fsw*, current amplitude *J*, and pulses duration Δ*tp*. (Δ*tp* = *d*/(*fsw**2), *d* being the duty cycle, in the range 5–95%). The maximum output current *J* is 1.2 A, and the maximum voltage is 11 kV. The frequency *fsw* can be varied from 80 kHz to 200 kHz. In order to control the rise of the reactor temperature, this supply is operated in "Burst mode" [1]: pulses trains are separated by power injection pauses; the durations of both bursts and pauses are fully controlled.

Side view images of the discharge are acquired by a digital camera (Logitech C920), with an interval of 20 s and an exposure time of 1/128 s. This camera is installed 40 cm from the axis of reactor and provides images such as the ones displayed in Figure 1. The area of interest is 28 mm high (outer diameter of the reactor) and 60 mm long (length of the metallic mesh). The camera acquires images with 2304 × 1536 pixels; once cropped for the area of interest, these values reduce to 437 × 248 (the difference in proportions results from a very slight misalignment of the camera with respect to the reactor axis). Despite such a device having an exposure time much longer than the lifetime of the streamers, as will be shown below, very interesting information concerning the distribution of the plasma can be drawn from the analysis of these images.

2.2. Image Processing Algorithm

The aim of the image processing is to calculate the β discharging ratio, which defines the surface covered by the plasma. The algorithm is achieved in two main steps:

- a geometrical transformation, which achieves a cylindrical projection.
- a segmentation process, used to calculate the surface of the area covered by the discharge.

The initial image captured by the camera (Figure 4) first receives basic manipulations, which makes the file lighter and speeds up further treatments.

First of all, the image is cropped (Figure 5a), so as to keep only the reactor (useful region) with the same dimensions as its side view: L width and 2.R height. Then, in order to reduce the size of the file containing the picture and speed up its manipulation, the true-color RGB image is converted into a grayscale image. Each element of the resulting matrix contains only the gray level, ranging from 0 to 255, calculated as a weighted sum of the corresponding red, green and blue pixels. The gray level (*GL*) is calculated with

the Python coded function (1), which implements recommendation Rec.709 [20]; these weights are considered to better represent human perception of red, green, and blue than equal weights.

$$GL = 0.2125 \times R + 0.7154 \times G + 0.0721 \times B \quad (1)$$

The obtained image is presented on Figure 5b; in all the pictures presented in this paper, for better readability, the grayscale images are shown with a color scale from violet (background), the lowest intensity, to yellow, the highest.

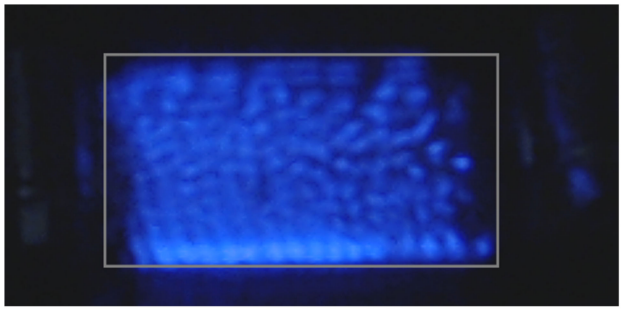

Figure 4. Initial image, acquired by the camera.

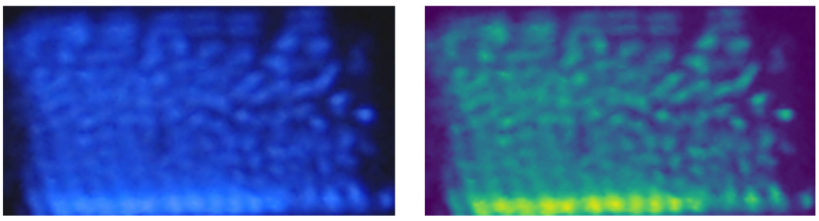

(**a**) (**b**)

Figure 5. Initial cropped image (**a**), and grayscale transformed (**b**).

2.2.1. Geometrical Transformation

The geometrical transformation is introduced in order to compensate the deformation of the discharge representation, which is caused by the cylindrical shape of the reactor, captured on the flat sensor of the camera. For that purpose, the Abel transformation [21–23] initially considered has been finally withdrawn, because the plasma distribution around the gas gap does not present the cylindrical invariance which is mandatory. A new method for calculation is proposed below.

On the taken image, the reactor cylindrical shape is flattened by the camera, as shown on Figure 6. The reactor has length L and is placed along the Z axis; the camera's optical axis is on the X axis. The plane (X, Y) is an orthogonal cross-section of the reactor (Figure 6b). The points $m(y_p)$ cover the external surface of the reactor, at outer radius r, for θ ranging from $-90°$ to $90°$. The point M(y), with y ranging from −R to +R, is the orthogonal projection, captured by the camera, of the points $m(y_p)$. Only the outer electrode is shown. Several geometrical assumptions are made:

(a) The streamer distribution is symmetrical to the plane X = 0 (the hidden face of the reactor is assumed to present the same aspect as the captured one). Therefore, only the front face is analyzed.
(b) The camera plane (Y, Z) is far enough from the reactor that the light rays reach it in parallel. This ensures that the points M(y) and $m(y_p)$ are aligned parallel to the optical axis of the camera (X axis). Therefore, the height of the image captured by the camera (Figure 6c) is equal to 2.R.
(c) Only the external surface of the reactor is considered—no depth of the plasma volume is considered (it means that possible streamers are seen as spots on the outer surface).

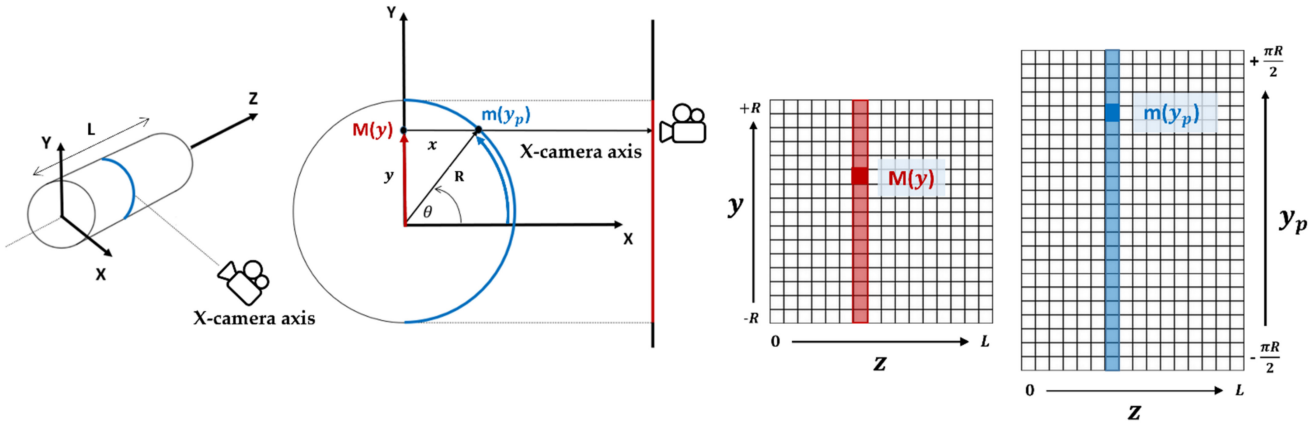

(**a**) (**b**) (**c**) (**d**)

Figure 6. Principle of the geometrical transformation (projection): (**a**) 3D view of the reactor and the camera. (**b**) Orthogonal cross-section of the reactor. (**c**) Acquired picture. (**d**) Transformed picture.

Starting from the captured image, the goal of the geometrical transformation is to build the projected output image (Figure 6d): it is the rollout of the DBD reactor external surface. The height ratio between the captured image (Figure 6c) and the projected one (Figure 6d) is therefore equal to $\pi/2$. The width is the same for both images and equal to the length L of the reactor.

In order to build Figure 6d, each M(y) point of the acquired image is used to define the $m(y_p)$ point at vertical position y_p; if a streamer appears on the original picture as a spot with $\Delta z \Delta y$ size, on the transformed image it is spanned into $\Delta z \Delta y_p$ with:

$$y_p = R \times \theta = R \times \sin^{-1}\left(\frac{y}{R}\right) \tag{2}$$

$$\Delta y_p = \frac{\Delta y \times R}{\sqrt{R^2 - y^2}} = \frac{\Delta y}{\cos(\theta)} \tag{3}$$

Equation (2) is obtained by a basic trigonometric manipulation: the length y_p, which is also a circle segment, is equal to the radius R multiplied by the θ angle. The ratio $\Delta y_p / \Delta y$ from Equation (3) is a first-order approximation obtained with first y-derivative of Equation (2). Using these equations, the image is projected to cylindrical coordinates and rolled out. This process is repeated along the Z axis in all planes (X, Y) of the reactor to obtain the full picture. Figure 7b shows the obtained image in cylindrical coordinates.

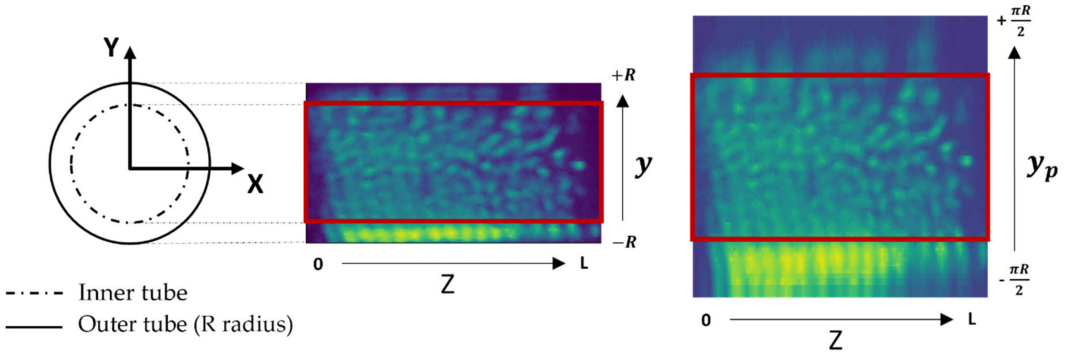

(**a**) (**b**)

Figure 7. Projected unrolled image of the outer surface of the reactor: (**a**) Acquired grayscale image—Cylindrical coordinates output image (**b**). Red rectangle highlights the inner tube of the reactor.

2.2.2. Image Segmentation

Step 1—area of interest: as can be seen in the unrolled picture Figure 7b, the lower and upper parts of the discharge look brighter than the central part of it. The coaxial geometry of the reactor and the transparent quartz walls cause this effect. In the central part of the discharge, the inner electrode creates a solid background for the pictures, whereas in the upper and lower parts, the gas gap between the two electrodes and quartz barriers produces an optical effect that intensifies the discharge. To avoid biased results due to this optical effect and according to the assumption (c) that the plasma volume has no depth, the image is cropped again, erasing the parts which do not present a solid background. They correspond to the gas gap and only the central part of the picture, which has the height of the diameter of the inner tube (red frame figure below), is kept (Figure 8b)—one should notice that this figure is different from the original one, Figure 7a.

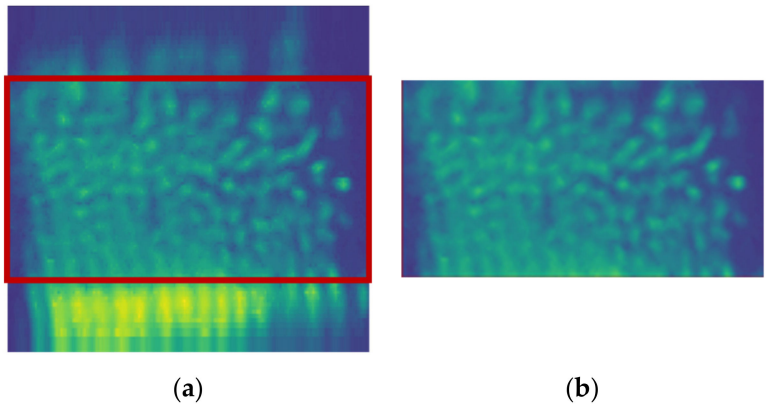

(**a**) (**b**)

Figure 8. Cylindrical coordinates output image (**a**), and its cropped central region with solid background (**b**).

Step 2—image segmentation: the discharge area is segmented using a thresholding technique, as shown in Figure 9. It means that a gray-level value called "threshold value" is used as the delimiter between the background and the discharge area. All pixels with values less than the threshold value are considered as background, and pixels with values greater than the threshold are considered as the discharge area. In order to find the threshold value, Otsu's method is used [24]: this method chooses a threshold value that minimizes the variance of the thresholded background and discharge pixels. The ability of this method to segment the image even with low intensity discharges (operating points at low power) of uniform appearance is remarkable (as will be shown in Section 3).

Figure 9. Segmented Discharge area (violet is background, yellow is discharge area).

Step 3—image analysis: the calculation of the β percentage is achieved with the ratio between the number of pixels of the discharge, obtained with the segmentation, and the total number of pixels. Other statistical results quantifying the discharge's uniformity are also presented in Section 3.3.

2.3. Partial Surface Discharging Analysis via the Electric Model

The DBD is commonly modelled in the literature by the electric circuit shown in Figure 10. C_d represents the capacitive behavior of the dielectric barrier(s), in this case the series equivalent capacitance of the two quartz cylinders. The gas is modeled as a dielectric (C_g) as long as it is not conductive ($|v_{gas}| < V\text{th}$, thus $i_{gas} = 0$), and after breakdown it is represented with a constant voltage ($v_{gas} = \pm V\text{th}$), the sign of which depends on the direction of the gas current [15,18,19].

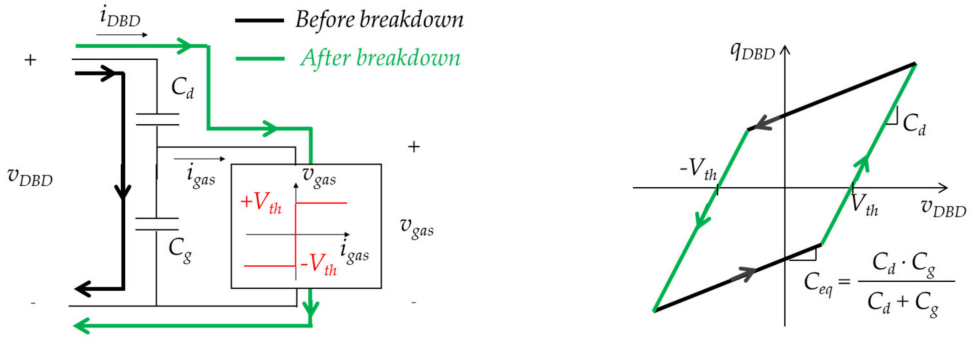

Figure 10. Simplified electric circuit model of the DBD, with current paths in ON–green and OFF–black plasma states (**a**) and its Manley's diagram (**b**).

The parameters of this model (C_d, C_g and Vth) are found with experimental waveforms for voltage and current on the DBD, then tracing the electrical charge vs. voltage diagram (known as Manley's diagram) as shown in Figure 10.

The slopes of the parallelogram are used to define the dielectric and series equivalent capacitances (respectively, C_d for the ON state and C_{eq} for the OFF state—C_{eq} being the value of the series connection of C_d and C_g). From the latter, the gas capacitance (C_g) is calculated. The zero-cross with the voltage axis determines the threshold voltage (Vth). The area enclosed by the parallelogram is equal to the energy injected during one period to the DBD, so it can be used to determine the average power.

It is well known that Vth, C_g, and C_d are physical parameters determined by the gas composition, pressure, dielectric material, and geometry; these three values define the behavior of the equivalent circuit, which remains predictive as long as the surface covered by the plasma on the electrodes, remains stable. Indeed, variations in the identified parameters as a function of the electric conditions given by the power supply are common, even if the reactor geometry does not change [11,12]. As shown in Figure 11, this can be observed in the case of the DBD reactor used in this work: here, the electrical energy injected into the plasma, controlled by the power supply, is changed. Accordingly, the discharge covers the whole surface of the reactor ((a), $\beta = 1$) or only part of it ((b), $\beta < 1$). Note that, concerning the identified parameters of the equivalent circuit (Figure 10), C_{eq} is similar for both cases, however, identified C_d and Vth change significantly: being physical parameters of the reactor, such changes are not acceptable.

As observed in the pictures beside the Manley's diagrams, this phenomenon in the model identification takes place when the discharge occurs in a partial area of the available electrode surface (Figure 11b). Depending on the operating conditions of the power supply, the discharge area extends until it fully covers the electrodes, and the values measured using Manley's diagram coincide with the theoretical ones. In that scenario, the classic DBD electric model, shown in Figure 10, completely represents the load. Nonetheless, for the partial surface discharging case, a modified model is proposed in the literature [8,11,25]. In consequence, a different equivalent electric model has to be used, where C_d, and C_g are both split into the non-discharging and discharging area (α and β percentages respectively, which fulfil: $\alpha + \beta = 1$), as displayed in Figure 12.

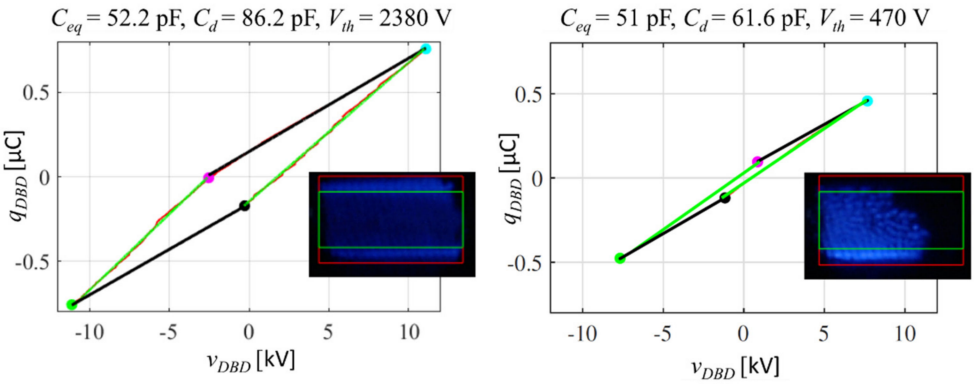

Figure 11. Change of the DBD identified model parameters (C_{eq}, C_d and Vth) for the same reactor, with different supply conditions, leading to different discharging ratio: β = 1 (**a**) and β < 1 (**b**).

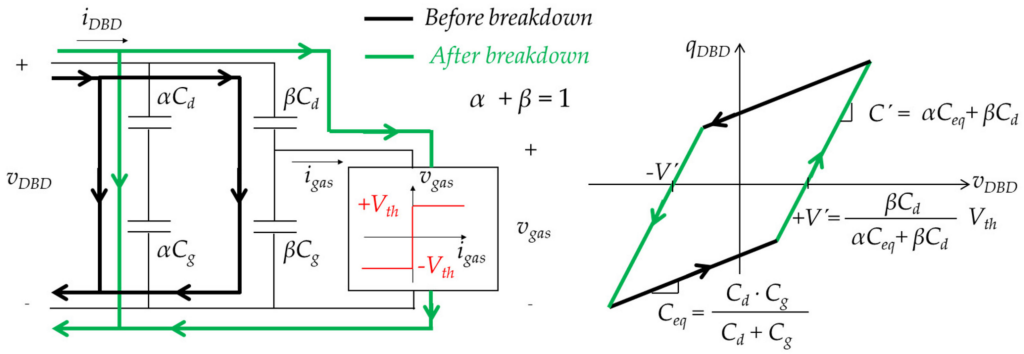

Figure 12. DBD electrical model for partial discharging area (**a**), proposed in [11], along with its modified Manley's diagram (**b**).

In this case, the α and β parameters are calculated having previously identified C_d, C_{eq}, C_g, and Vth, using the Manley's diagram for a discharge covering all the surface. For the partial discharging area condition, C_{eq} does not change, as the series capacitor of the two equivalent circuits is the same when there is no discharge (Figures 10 and 12): this is proven experimentally in the example of Figure 11, with an error below 2.4% between the two measurements.

The percentage of the discharge area (β) can be found with the slope when the discharge has been established (C'), as follows:

$$\beta = \frac{C' - C_{eq}}{C_d - C_{eq}} \tag{4}$$

The breakdown voltage, Vth, can be verified according to Equation (5), using the charge variation in the OFF state, $\Delta Qdbd_{OFF}$ (black segments on Figure 12)

$$V\text{th} = \frac{\Delta Qdbd_{OFF}}{2 \times C_g}, \text{OFF state} \tag{5}$$

3. Results

The application of the two diagnostic methods for β discharging ratio, described in the previous section, is now presented and discussed.

3.1. Agreement of the Circuit Analysis Method and Image Processing for β Ratio Diagnostic

Two operating points obtained at 5 kHz with the sine voltage generator, corresponding to two different power levels (10 W and 25 W), are selected. Figure 13 presents the obtained results in each column (top-down): the electrical waveforms (voltage—blue, and current—green), the Manley diagram build with these data, the acquired reactor's pictures, the segmented and cropped (area of interest) grayscale image together with the β discharging ratio obtained from the equivalent circuit approach and with the image processing. The last data is associated with the margin error (the difference between the maximum and minimum values) estimated through repeated calculations using three different images acquired in steady state conditions (see below) during three different experiments.

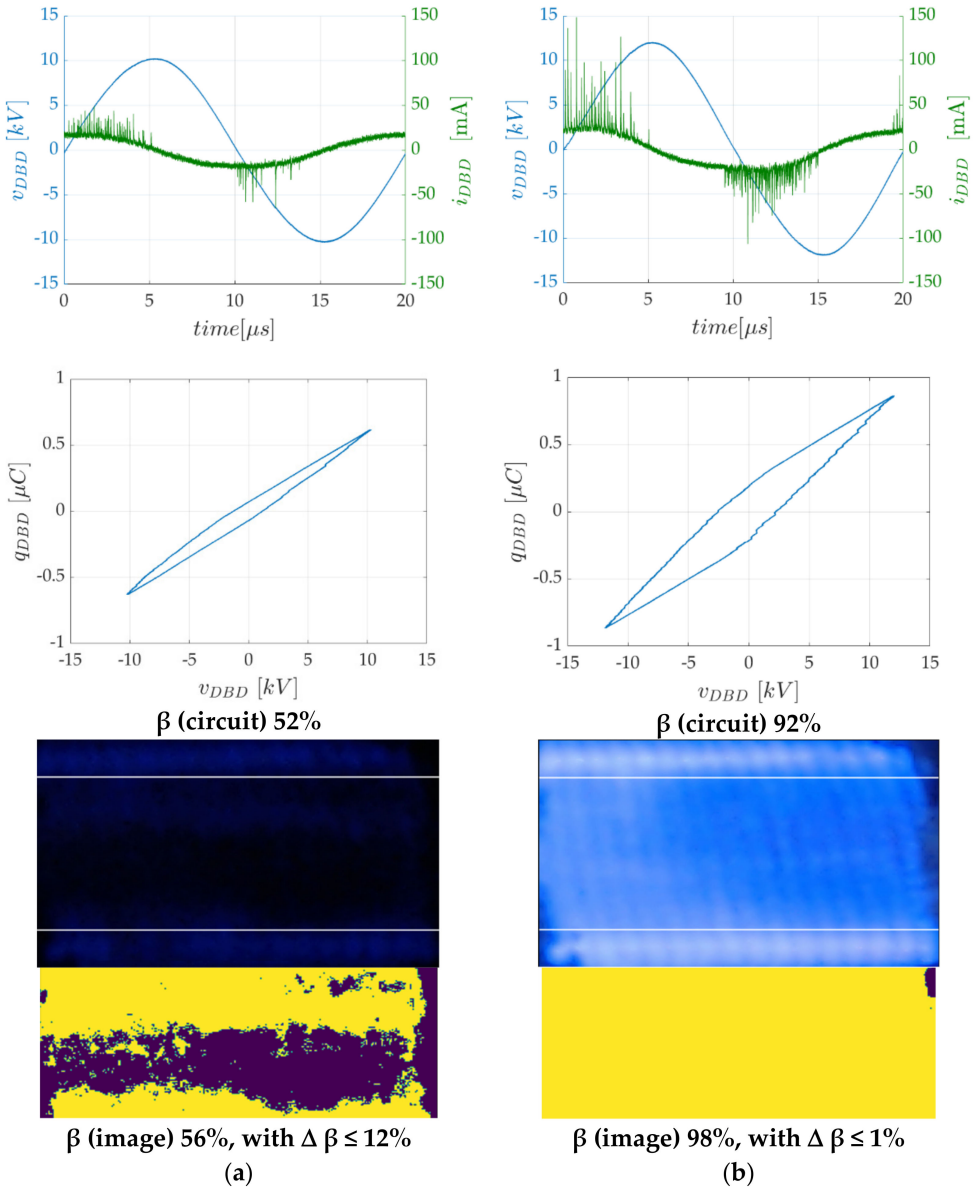

Figure 13. Application of both diagnostic methods: (**a**) low power level (10 W). (**b**) high power (25 W). Measures are acquired in steady state.

It should be mentioned that the coverage of the discharge area varies from the time the system is started, with a typical transient shown in Figure 14. Here, the record starts when the power supply is turned ON, with a gas flow already stabilized (see Figure 2). For the presented operating conditions (f = 10 kHz, P = 30 W), one can observe during the

transient the rise of the discharging surface (and accordingly the β ratio), which definitively stabilizes only after approximatively 120 s. For steady-state process analyses, data should only be acquired after this system time constant.

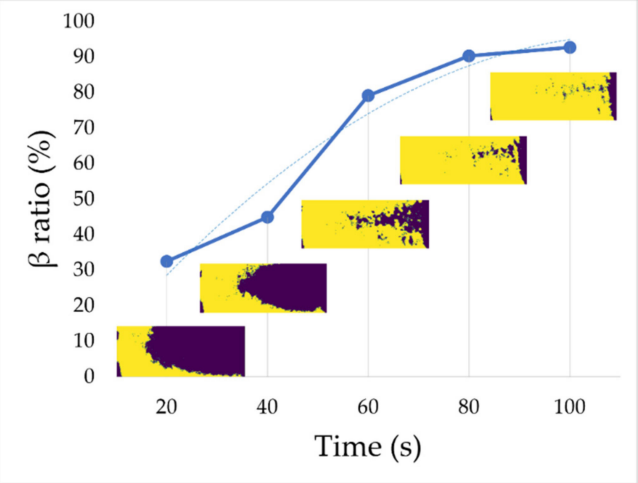

Figure 14. Partial discharging ratio β variation during the startup transient.

The two methods described in the previous section are now applied on a set of measures acquired with operating points covering a large domain (sine voltage power supply). This diversity of considered conditions is aimed at comparing the results of the two methods, whose results are presented on Figure 15: for each operating condition, three measurements are acquired in steady state during different experiments. The displayed value is the average of these three results, and the error bar indicates the maximum and minimum values. One can notice the very good agreement with a difference which remains generally below 10%. In most cases, the β discharging ratio obtained with the electrical circuit approach remains in the error range of the image processing method. The latter is obtained, using several images repeatedly acquired for each operating point; this systematic uncertainty remains below 12%.

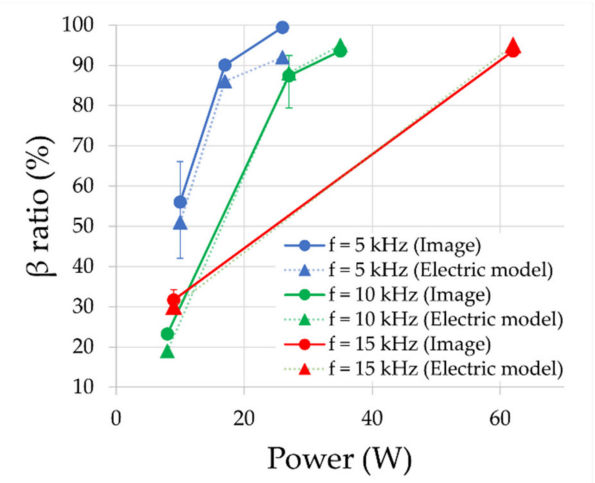

Figure 15. Partial discharging ratio β obtained with image processing and equivalent circuit analyzes. Results are grouped by values of supply frequency; adjustments of injected power are achieved with the peak value of imposed v_{DBD} voltage. Displayed values are obtained in steady state.

3.2. Application to Rectangular Current Power Supply Operated in Burst Mode

As shown in Figure 16, results obtained with the rectangular current power supply are difficult to analyze through the equivalent circuit approach: indeed, each burst of

current pulses injected into the DBD creates an electrical transient (see voltage and current waveforms on Figure 16a), which has no time to vanish before the end of the burst. As a result, the Q-V Manley diagram exhibits a poorly trapezoidal shape, as can be appreciated in Figure 16b: this makes it very difficult to select the slopes to be used for the calculation of the circuit's parameters.

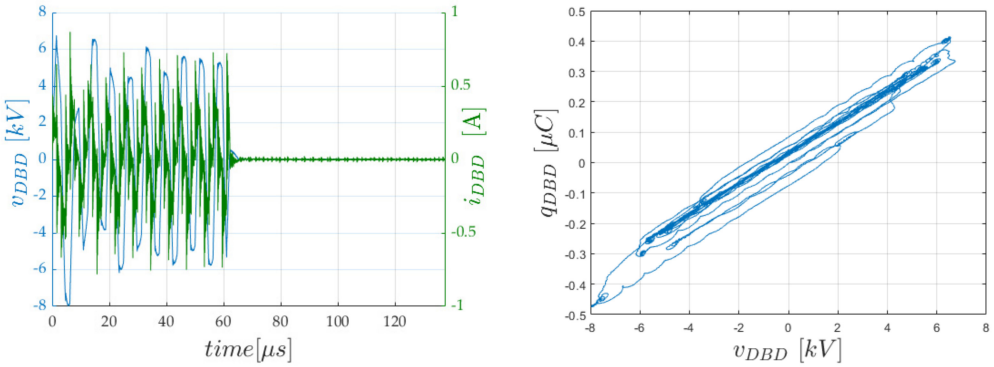

(**a**) (**b**)

Figure 16. Rectangular current supplied system: electrical measurements of a whole burst (**a**), with DBD voltage (blue) and current (green), and associated Q-V Manley diagram (**b**).

Taking advantage of the very good convergence of both methods for β ratio diagnostic highlighted on Figure 15, it is proposed to admit:

- the parameter set (C_d, C_g, Vth), acquired thanks to previously achieved experiment, where the discharge fully covers the surface of the reactor (β = 100%), sketched by the equivalent circuit of Figure 10;
- the β ratio obtained by the image processing.

Using Equations (4) and (5), which translate the behavior of the equivalent circuit of Figure 12, it becomes possible to build and to draw the parallelepipedal figure, which should be considered.

Note that the image acquisition shows an averaged behavior of the system. As for the β value provided by the analysis of this image, therefore, this approach provides an equivalent average behavior over the burst. The image processing of the acquired picture shown in Figure 17a gives: β = 56%. Together with already known circuit parameters (C_d = 90 pF, C_g = 135 pF, Vth = 2585 V, independent from operating conditions), Figure 17b shows the Manley figure (red).

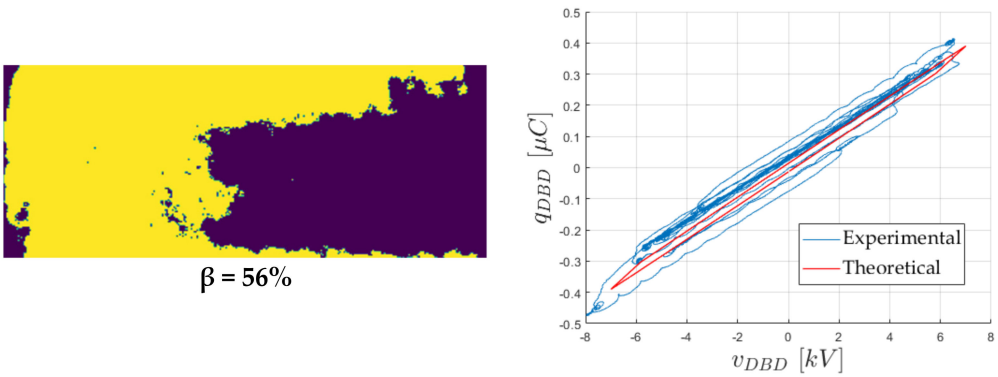

(**a**) (**b**)

Figure 17. Rectangular current supplied system: processed image corresponding to Figure 16 (**a**), giving a value: β = 56% experimental Manley diagram (**b**), blue and the theoretical one (red), obtained with the known parameter set for the equivalent circuit: C_d = 90 pF, C_g = 135 pF, Vth = 2585 V.

3.3. Effect of the Supply Waveform on the Discharge Uniformity: Additional Diagnostic Provided by the Image Processing

In addition to the segmentation process, other statistical diagnostics of the images can provide very useful information about the discharge. We now consider the operating conditions obtained with the electrical waveforms shown in Figure 3, with two different generators; the waveforms are completely different but, in fact, they have the same power level (approx. 40 W).

The appearance of the discharges [26] shown in Figure 18 are very different: the discharge obtained with the sinusoidal voltage source (column (b)) appears much more diffuse than the one pumped with the rectangular current source (column (a)): in the original picture (column (a)), the spots which can be related to the streamers are clearly visible.

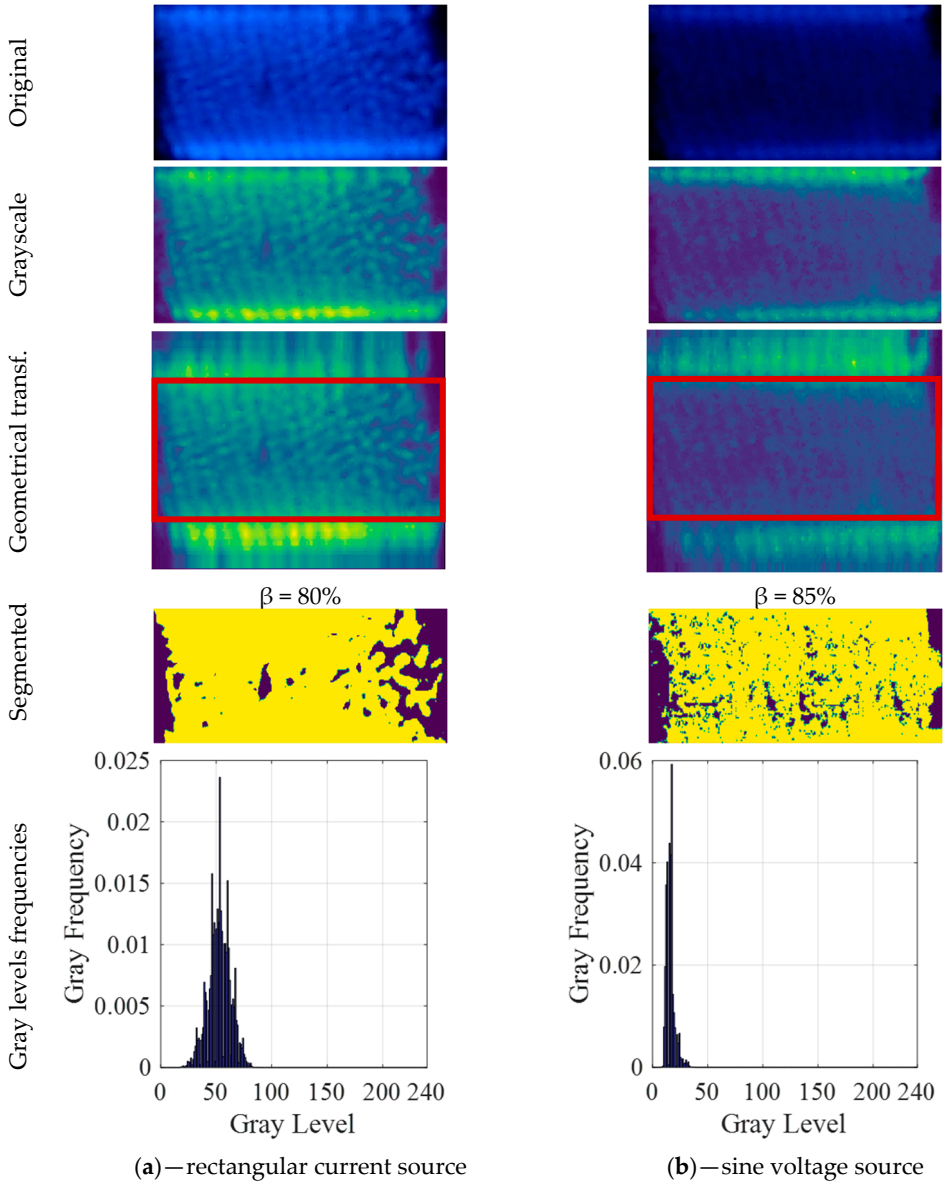

Figure 18. Image diagnostic of operating conditions obtained with square current source (column (**a**)) and sine voltage power supply (column (**b**))—electrical waveforms presented in Figure 3—from top to bottom: original image, grayscale, result of geometrical transformation, segmented image (central area), gray levels frequency.

The gray-levels histograms of the last row in Figure 18 present the result of a statistical analysis, which presents good matching with the discharge appearance and offers a quantification solution to translate the visual effect into a number. This analysis was proposed by [13] and is achieved as previously on the only central part of the image (red frame); it is carried out after the translation of the image into gray levels and its geometrical transformation (before the segmentation): the horizontal axis of the histogram presents the gray level (from 0 to 255), and the vertical axis presents the frequency of pixels for each level. Based on the histogram results, statistical measures as the mean gray level and the standard deviation are used to characterize the discharge. Below, the parameters of this analysis are commented:

- Mean Gray Level (μgray): It is the mean of the gray-level value (in the central discharge area). This indicates the mean brightness of the discharge. In order to be able to compare the discharges obtained under different operating conditions, care must be taken to deactivate all automatic settings of the camera.
- Gray Level Intensity: It is the sum of the gray-level values of the pixels in the area of interest.
- Discharge Intensity/mm^2: It is the Gray Level Intensity divided by the area covered by the discharge.
- Standard Deviation (SD): the SD measures the dispersion of the data from its mean value, and it is a crucial parameter to determine the discharge uniformity quantitatively [27]. In an ideal uniform discharge, all the reactor pixels should have the same gray-level value; thus, the SD is zero in this case. The SD value will rise if the gray level takes increasingly different values on the surface. In general, the lower the standard deviation, the data points tend to be closer to their mean, meaning a more uniform discharge. The value of SD is calculated considering each pixel of the image, as defined in [27].

Table 1 presents the resulting parameters of the image processing for both cases shown in Figure 18.

Table 1. Grayscale images statistical properties (electrical waveforms presented on Figure 3 and images in Figure 18).

Pict.	β [%]	Discharge Area [mm^2]	Mean Gray Level—μgray	Gray Level Intensity	Gray Level Intensity/mm^2	Standard Deviation—SD
Rectangular current—column (a)	80	1659	52.73	1,787,099	1077	10.12
Sinusoidal voltage—column (b)	85	1762	15.83	576,172	327	3.88

As can be seen, the SD of the case obtained with the rectangular current source is significantly higher than cases with the sine voltage. Despite the fact that cases worked with similar electrical power, the intensity of the first case is higher than for the second. Accordingly, the discharges obtained by the sinusoidal voltage source are more uniform, diffuse, and weak than the discharges obtained by the square current source. This observation has been verified with a set of different operating points in a wide range of the β parameter.

The Manley figures of both supply conditions showed that DBD works in a filamentary mode, even if diffuse and uniform discharges appeared with the sinusoidal voltage source.

One can notice that the image (a) is much more luminous than the (b) one—this is confirmed by the difference of the values of the Gray level Intensity/mm^2. Nevertheless, the Otsu's algorithm has been clearly able to differentiate the background and the area covered by the discharge. In this way, the discharge segmentation process is validated under different image conditions.

4. Conclusions

Two methods to evaluate the β discharging ratio of a dielectric barrier discharge are proposed in this paper. The equivalent circuit-based method uses recorded waveforms of voltage and current of the DBD reactor to build the Manley's diagram and to identify the equivalent circuit parameters and the β ratio. The image processing method uses pictures of the discharge captured through the transparent walls of the reactor. A two-step algorithm is presented and validated. First, a geometrical transformation compensates the distortion due to the shape of the reactor. Second, the segmentation of the images based on the Otsu's method is used to identify the discharge area and then to analyze it, based on the gray-level histograms.

These two methods were proved to work very well and to provide remarkably coherent results, under different intensity conditions of the discharge, when pumped with different electrical waveforms obtained with two very different power supplies. Additionally, a comparison between the discharges produced by a square current source and a sinusoidal voltage source with similar power levels has shown that more uniform discharges are obtained with the sinusoidal voltage source, and more intense discharges are obtained with the square current source. These observations have been correlated with statistical properties of the gray level acquired images, which provide a quantified appreciation of the discharge uniformity, very useful for achieving the comparison of the performances.

Author Contributions: Conceptualization, R.D. and H.P.; Investigation, V.R., R.D., N.B. and H.P.; Software, V.R. and N.B.; Supervision, R.D. and H.P.; Validation, V.R.; Visualization, V.R. and N.B.; Writing—original draft, V.R., R.D. and H.P.; Writing—review & editing, R.D., N.B. and H.P. All authors have read and agreed to the published version of the manuscript.

Funding: This research received no external funding.

Data Availability Statement: Not applicable.

Acknowledgments: The authors thank the French-Colombian cooperation program ECOS Nord—Colciencias-ICETEX, as well as Javeriana University project 10035.

Conflicts of Interest: The authors declare no conflict of interest.

References

1. Kogelschatz, U. Dielectric-barrier discharges: Their History, Discharge Physics, and Industrial Applications. *Plasma Chem. Plasma Process.* **2003**, *23*, 1–46. [CrossRef]
2. Massines, F.; Sarra-Bournet, C.; Fanelli, F.; Naudé, N.; Gherardi, N. Atmospheric Pressure Low Temperature Direct Plasma Technology: Status and Challenges for Thin Film Deposition. *Plasma Process. Polym.* **2012**, *9*, 1041–1073. [CrossRef]
3. Fridman, G.; Friedman, G.; Gutsol, A.; Shekhter, A.B.; Vasilets, V.N.; Fridman, A. Applied Plasma Medicine. *Plasma Process. Polym.* **2008**, *5*, 503–533. [CrossRef]
4. Ivankov, A.; Capela, T.; Rueda, V.; Bru, E.; Piquet, H.; Schitz, D.; Florez, D.; Diez, R. Experimental Study of a Nonthermal DBD-Driven Plasma Jet System Using Different Supply Methods. *Plasma* **2022**, *5*, 75–97. [CrossRef]
5. Wiesner, A.; Diez, R.; Florez, D.; Piquet, H. System for experimental investigation of DBD excilamps in view of control and optimization of UV emission. *Math. Comput. Simul.* **2019**, *165*, 92–106. [CrossRef]
6. Lomaev, M.I.; Sosnin, E.A.; Tarasenko, V.F.; Shits, D.V.; Skakun, V.S.; Erofeev, M.V.; Lisenko, A.A. Capacitive and barrier discharge excilamps and their applications (Review). *Instrum. Exp. Tech.* **2006**, *49*, 595–616. [CrossRef]
7. Talebizadeh, P.; Babaie, M.; Brown, R.; Rahimzadeh, H.; Ristovski, Z.; Arai, M. The role of non-thermal plasma technique in NOx treatment: A review. *Renew. Sustain. Energy Rev.* **2014**, *40*, 886–901. [CrossRef]
8. Fang, Z.; Qiu, Y.; Zhang, C.; Kuffel, E. Factors influencing the existence of the homogeneous dielectric barrier discharge in air at atmospheric pressure. *J. Phys. D Appl. Phys.* **2007**, *40*, 1401–1407. [CrossRef]
9. Okazaki, S.; Kogoma, M.; Ueharaÿ, M.; Kimura, Y. Appearance of stable glow discharge in air, argon, oxygen and nitrogen at atmospheric pressure using a 50 Hz source. *J. Phys. D Appl. Phys.* **1993**, *26*, 889–892. [CrossRef]
10. Belinger, A.; Naudé, N.; Ghérardi, N. Transition from diffuse to self-organized discharge in a high frequency dielectric barrier discharge. *Eur. Phys. J. Appl. Phys.* **2017**, *79*, 10802. [CrossRef]
11. Peeters, F.J.J.; van de Sanden, M.C.M. The influence of partial surface discharging on the electrical characterization of DBDs. *Plasma Sources Sci. Technol.* **2014**, *24*, 015016. [CrossRef]
12. Peeters, F.; Butterworth, T. Electrical Diagnostics of Dielectric Barrier Discharges. In *Atmospheric Pressure Plasma-from Diagnostics to Applications*; IntechOpen: London, UK, 2018. [CrossRef]

13. Wu, Y.; Ye, Q.; Li, X.; Tan, D. Classification of dielectric barrier discharges using digital image processing technology. *IEEE Trans. Plasma Sci.* **2012**, *40*, 1371–1379. [CrossRef]
14. Manley, T.C. The Electric Characteristics of the Ozonator Discharge. *Trans. Electrochem. Soc.* **1943**, *84*, 83–96. [CrossRef]
15. Pipa, A.; Brandenburg, R. The Equivalent Circuit Approach for the Electrical Diagnostics of Dielectric Barrier Discharges: The Classical Theory and Recent Developments. *Atoms* **2019**, *7*, 14. [CrossRef]
16. Kriegseis, J.; Moller, B.; Grundman, S.; Tropea, C. Capacitance and power consumption quantification of dielectric barrier discharge (DBD) plasma actuators. *J. Electrost.* **2011**, *69*, 302–312. [CrossRef]
17. Dubois, J. EMI/RFI Shielding Products & Smart Electronics Systems. Available online: https://www.jacquesdubois.com/ (accessed on 1 August 2022).
18. Rueda, V.; Wiesner, A.; Diez, R.; Piquet, H. Power Estimation of a Current Supplied DBD Considering the Transformer Parasitic Elements. *IEEE Trans. Ind. Appl.* **2019**, *55*, 6567–6575. [CrossRef]
19. Florez, D.; Schitz, D.; Piquet, H.; Diez, R. Efficiency of an Exciplex DBD Lamp Excited Under Different Methods. *IEEE Trans. Plasma Sci.* **2018**, *46*, 140–147. [CrossRef]
20. The International Telecommunication Union. *Basic Parameter Values for the HDTV Standard for the Studio and for International Programme Exchange*; ITU-R Recommendation BT.709, [formerly CCIR Rec. 709]; The International Telecommunication Union: Geneva, Switzerland, 1990.
21. van der Schans, M. Characterization of a Dielectric Barrier Discharge with a Square Mesh Electrode. Master's Thesis, Eindhoven University of Technology, Department of Applied Physics, Eindhoven, The Netherlands, 2014. Available online: https://pure.tue.nl/ws/portalfiles/portal/46997630/784532-1.pdf (accessed on 1 August 2022).
22. Keefer, D.R.; Smith, L.M.; Sudharsanan, S.I. Abel inversion using transform techniques. In Proceedings of the International Congress on Applications of Lasers & Electro-Optics, Arlington, VA, USA, 10–13 November 1986; pp. 50–58. [CrossRef]
23. Dribinski, V.; Ossadtchi, A.; Mandelshtam, V.A.; Reisler, H. Reconstruction of Abel-transformable images: The Gaussian basis-set expansion Abel transform method. *Rev. Sci. Instrum.* **2002**, *73*, 2634–2642. [CrossRef]
24. Otsu, N. A Threshold Selection Method from Gray-Level Histograms. *IEEE Trans. Syst. Man. Cybern.* **1979**, *9*, 62–66. [CrossRef]
25. Zhang, Q.; Zhao, H.; Lin, H.; Wu, J. A Novel Electrical Model of Dielectric Barrier Discharge for Quasi-Homogeneous Mode and Filamentary Mode. In Proceedings of the 21st International Conference on Electrical Machines and Systems (ICEMS), Jeju, Korea, 7–10 October 2018; pp. 865–870. [CrossRef]
26. Radu, I.; Bartnikas, R.; Wertheimer, M.R. Frequency and Voltage Dependence of Glow and Pseudoglow Discharges in Helium Under Atmospheric Pressure. *IEEE Trans. Plasma Sci.* **2003**, *31*, 1363–1378. [CrossRef]
27. Ye, Q.; Yun, D.; Yang, F.; Tan, D. Application of the gray-level standard deviation in the analysis of the uniformity of DBD caused by the rotary electrode. *IEEE Trans. Plasma Sci.* **2013**, *41*, 540–544. [CrossRef]